

ORIGINAL ARTICLE

Next-generation pathology detection of T cell–antigen-presenting cell immune synapses in human liver allografts

Michelle A. Wood-Trageser¹  | Drew Lesniak¹ | Alessandro Gambella^{1,2}  |
 Kayla Golnoski¹ | Sandy Feng³  | John Bucuvalas⁴  |
 Alberto Sanchez-Fueyo⁵  | A. Jake Demetris¹ 

¹Division of Liver and Transplant Pathology, University of Pittsburgh, Pittsburgh, Pennsylvania, USA

²Pathology Unit, Department of Medical Sciences, University of Turin, Torino, Italy

³Division of Transplantation, Department of Surgery, University of California San Francisco, San Francisco, California, USA

⁴Mount Sinai Kravis Children's Hospital and Recanati/Miller Transplantation Institute, Mount Sinai Health System, New York, New York, USA

⁵Institute of Liver Studies, King's College London, London, UK

Correspondence

A. Jake Demetris, UPMC Montefiore Hospital, Room E741, 3459 5 Avenue, Pittsburgh, PA 15213, USA.
 Email: demetrisaj@upmc.edu

Funding information

Division of Intramural Research, National Institute of Allergy and Infectious Diseases, Grant/Award Number: U01-AI-100807 and UM1AI109565; Immune Tolerance Network; National Institute of Diabetes and Digestive and Kidney Diseases, Grant/Award Number: R01 DK114180; University of Pittsburgh

Abstract

Background and Aims: In otherwise near-normal appearing biopsies by routine light microscopy, next-generation pathology (NGP) detected close pairings (immune pairs; iPAIRs) between lymphocytes and antigen-presenting cells (APCs) that predicted immunosuppression weaning failure in pediatric liver transplant (LTx) recipients (Immunosuppression Withdrawal for Stable Pediatric Liver Transplant Recipients [iWITH], NCT01638559). We hypothesized that NGP-detected iPAIRs enrich for true immune synapses, as determined by nuclear shape metrics, intercellular distances, and supramolecular activation complex (SMAC) formation.

Approach and Results: Intralobular iPAIRs (CD45^{high} lymphocyte–major histocompatibility complex II⁺ APC pairs; $n = 1167$, training set) were identified at low resolution from multiplex immunohistochemistry–stained liver biopsy slides from several multicenter LTx immunosuppression titration clinical trials (iWITH; NCT02474199 (Donor Alloantigen Reactive Tregs (darTregs) for Calcineurin Inhibitor (CNI) Reduction (ARTEMIS); Prospective Longitudinal Study of iWITH Screen Failures Secondary to Histopathology). After excluding complex multicellular aggregates, high-resolution imaging was used to examine immune synapse formation ($n = 998$). By enriching for close intranuclear lymphocyte–APC distance (mean: 0.713 μm) and lymphocyte nuclear flattening (mean ferret diameter: 2.1), SMAC formation was detected in 29% of iPAIR-engaged versus 9.5% of unpaired lymphocytes. Integration of these morphometrics enhanced NGP detection of immune synapses (ai-iSYN). Using iWITH preweaning biopsies from eligible patients ($n = 53$; 18 tolerant, 35 nontolerant; testing set), ai-iSYN accurately predicted (87.3% accuracy vs. 81.4% for iPAIRs; 100% sensitivity, 75% specificity) immunosuppression

Abbreviations: ai-iSYN, automated imaging detection for immune synapses; APC, antigen-presenting cell; ARTEMIS, Donor Alloantigen Reactive Tregs for Calcineurin Inhibitor Reduction clinical trial; DSA, donor-specific antibody; FFPE, formalin-fixed, paraffin-embedded; HiRes, high-resolution; iPAIR, software-identified immune pairing; IS, immunosuppression; ISM, immunosuppression minimization; ISW, immunosuppression withdrawal; iWITH, Immunosuppression Withdrawal for Stable Pediatric Liver Transplant Recipients clinical trial; iWITH-IN, Prospective Longitudinal Study of iWITH Screen Failures Secondary to Histopathology clinical study; LoRes, low-resolution; LTx, liver transplant; NGP, next-generation pathology; SMAC, supramolecular activation complex; TCMR, T cell–mediated rejection; WSI, whole slide imaging.

weaning failure. This confirmed the presence and importance of *intra*lobular immune synapse formation in liver allografts. Stratification of biopsy mRNA expression data by immune synapse quantity yielded the top 20 genes involved in T cell activation and immune synapse formation and stability.

Conclusions: NGP-detected immune synapses (subpathological rejection) in LTx patients prior to immunosuppression reduction suggests that NGP-detected (allo)immune activity usefulness for titration of immunosuppressive therapy in various settings.

INTRODUCTION

Understanding the pathophysiological mechanisms of liver allograft injury and eventual rejection versus allograft acceptance (reviewed in Wood-Trageser et al.^[1,2]) is predicated in studies of immune activity in the hepatic lobules.^[3–6] Immune synapses result when antigen is presented to lymphocytes from hematopoietic-derived antigen-presenting cells (APCs; reviewed in Guadino and Kumar^[7] and Garcia and Ismail^[8]). Specifically, prior observations of T cell interactions with APCs in liver revealed that (a) intrahepatic T cell priming occurs primarily, but not exclusively, via Kupffer cells in experimental animal models^[5]; (b) gene expression studies of liver transplant (LTx) recipients who failed immunosuppression (IS) withdrawal (ISW) showed upregulation of “antigen presentation” gene pathways^[9]; (c) a lower density of lobular CD8⁺ cells predict successful ISW^[3,4]; and (d) CD8⁺ effector T cells drive T cell-mediated rejection (TCMR) after ISW.^[10] Based on lymphocyte flattening and supramolecular activation complex (SMAC) formation at the point of contact between a T cell and an APC,^[11–15] immune synapses can be morphologically defined when imaged experimentally using high-resolution (HiRes) microscopy,^[16–20] live cell imaging,^[13,21,22] or flow cytometry.^[23] However, relatively few groups have attempted to evaluate immune synapses in human formalin-fixed, paraffin-embedded (FFPE)^[4,9,11,12,24–27] or frozen tissue specimens.^[28,29] Next-generation pathology (NGP) is defined as automated multiplex immunohistochemistry (mIHC) followed by whole slide imaging (WSI) and automated image analysis.^[1] NGP offers a practical approach to link observations from experimental animal models to human liver allograft biopsies.

ISW trials highlight the need for assays to guide effective IS titration to maintain allograft health in a quiescent immune environment through a personalized approach to IS management.^[2,4] We studied biopsies collected from a multicenter cohort of pediatric LTx recipients, performed to determine eligibility for enrollment into an ISW trial (NCT01638559). Routine histopathological findings (i.e., hematoxylin and eosin or trichrome stains) categorized patients into distinct

clusters based on the presence or absence of allograft inflammation with tissue damage—early warning signs of an active alloimmune response.^[4,9,30] The three clusters had transcriptional profiles consistent with (1) relatively stable or “normal” grafts (e.g., Ishak fibrosis stage 0–1, none to mild perivenular fibrosis), (2) grafts experiencing low-grade subclinical TCMR, or (3) grafts exhibiting predominantly pathological fibrosis with/without inflammation.^[9] Interrogation of the liver immune microenvironment via NGP in biopsies from children who initiated ISW predicted successful ISW with 94% sensitivity and 66% specificity.^[4] Failed ISW was characterized by increased density of (a) lobular lymphocytes spatially close (within 5 μ m) to APCs (i.e., “immune pairs” [iPAIRS]); (b) MAC387⁺ cells; and (c) CD8⁺ T cells.^[4,9] NGP exposed a spectrum of allograft inflammation within the intrahepatic microenvironment that was not apparent via routine histopathological assessment.^[2,9] Detected iPAIRs were hypothesized to represent immune synapse-mediated indirect or semi-direct intrahepatic alloantigen presentation because recipient Kupffer cells largely replace donor ones.^[10,31] Despite calls for noninvasive allograft monitoring and contrary to the 2018 consensus statement of IS minimization (ISM) in LTx recipients,^[32] the above findings show that biochemical monitoring alone was insufficient to capture subclinical allograft injury processes.

This study (Figure 1) was undertaken to determine if automated detection of iPAIRs represent “true immune synapses.” Instead of simple staining positivity and close spatial proximity, we used independent nuclear shape changes and SMAC formation to define immune synapses. We then used a refined computer-assisted identification method for use on low-resolution (LoRes) images, most applicable to clinical laboratories. Additionally, gene expression in biopsies, supervised via increasing numbers of immune synapses, was queried to identify signaling pathways that correspond to the development of alloimmune effector mechanisms via activation of immune synapses. This has the potential to advance our understanding of the underlying afferent immunopathological mechanisms leading to graft rejection and subsequent deterioration of graft structure. As a quality assurance exercise, we

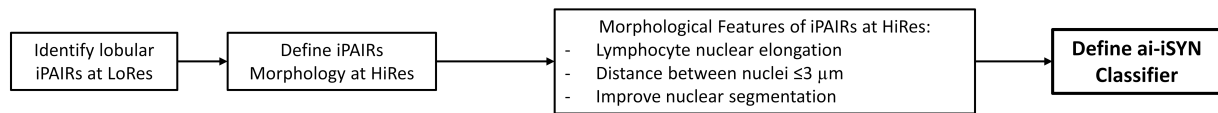
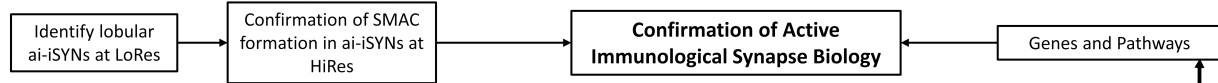
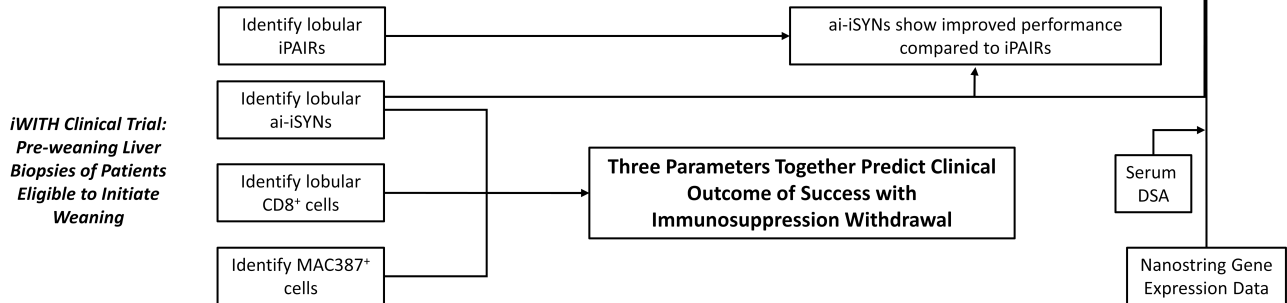
(A) MORPHOLOGICAL PHENOTYPING OF SOFTWARE-IDENTIFIED iPAIRS**(B) CONFIRMATION OF IMMUNE SYNAPSE BIOLOGY in SOFTWARE IDENTIFIED ai-iSYNs****(C) PERFORMANCE CONFIRMATION IN A CLINICAL COHORT**

FIGURE 1 Workflow for refinement of Automated Image detection of Immune SYNapses (ai-iSYN) classifier, confirmation of active immune synapse biology, and confirmation of prediction model in a clinical cohort. A three-step approach was used to define software-assisted identification of immune synapses detected on low-resolution (LoRes) imaging, confirm its biological relevance, and incorporation of the method into a larger, clinically applicable prediction algorithm for prediction of successful immunosuppression withdrawal. (A) First, images from our repository of clinical trials were used to evaluate the morphological characteristics of the lymphocyte ($CD45^{\text{high}}$) in computer-assisted identified lobular immune pairs (iPAIRs) with an antigen-presenting cells ($MHCII^{\text{only}}$). High-resolution (HiRes) imaging of iPAIRs was used to gather cytoplasmic (Figure S5) and nuclear data (Figure S6) that enabled refinement of the new classifier, ai-iSYN (Figure 2A). (B) Biological definitions of immune synapses were queried using cellular polarization (supramolecular activation complex [SMAC] formation) as a surrogate for stable immune synapse formation (Figure 2B, C) and gene expression enrichment for pathways related to active immune synapses (Figure 3, Table 1). Ai-iSYNs ($CD34^{\text{+}}/CD3^{\text{+}}/CD45^{\text{+}}/MHCII^{\pm}$ cells paired with $MHCII^{\text{only}}$ cells) were visualized to determine if lymphocytes in these computer-identified pairs displayed SMACs. The ai-iSYN classifier was applied to the existing iWITH dataset of pediatric baseline eligibility biopsies, and the number of lobular ai-iSYNs per square millimeter was used to inform the analysis of the existing gene expression data for signatures related to immune synapse formation and queried for relationships to donor-specific antibody (DSA) values. (C) To show clinical application, the refined classifier for lobular ai-iSYN, lobular $CD8^{\text{+}}$ cells (Figure S9), and $MAC387^{\text{+}}$ cells, markers of an inflamed liver immune microenvironment, were used as three parameters of a prediction algorithm for determining success after immunosuppression withdrawal using iWITH trial specimens as a confirmation cohort (Figure 4).

then tested the performance of our refined automated detection method to predict successful ISW, revealing a spectrum of quiescent to activated biopsies based on the liver immune milieu.

METHODS

Specimens and clinical data

FFPE specimens (and associated clinical meta-data) were collected from patients consented under two multicenter clinical trials focused on ISM or ISW: (1) Immunosuppression Withdrawal for Stable Pediatric Liver Transplant Recipients (iWITH, NCT01638559)^[4,9] and (2) Donor Alloantigen Reactive Tregs for Calcineurin Inhibitor Reduction (ARTEMIS, NCT02474199); and one multicenter study: (3) Prospective Longitudinal Study of iWITH Screen Failures Secondary to

Histopathology (iWITH-IN). Available leftover tissues were randomly selected for use as approved by the University of Pittsburgh Institutional Review Board office under PRO11090600 and/or STUDY19010225 where informed consent was waived. No additional patients were consented explicitly for this study and no additional tissues were collected. No donor organs were obtained from executed prisoners or institutionalized persons for the purposes of this study.

Immunohistochemistry and Imaging

Staining for $CD45$ /major histocompatibility complex II ($MHCII$)/ $CD34$, $MAC387$, and $CD8$ on iWITH specimens was conducted as previously described.^[4,9] Staining for $CD34/CD45/CD3/MHCII/CD8$ and comparisons between staining methodologies and staining consistency (Figure S1) is provided in the Supporting Methods.

For antibody information see Table S1. LoRes imaging (0.325 μm per pixel) was performed on a Zeiss Axioscan Z.1, and HiRes imaging (0.06 μm per pixel) was performed on a Zeiss AxioImager M2 Motorized Microscope.

Characterization of lobular iPAIRs using HiRes, in-depth morphological analysis

Categorization

Lobular iPAIRs per mm^2 was the most significant parameter in our operational tolerance prediction algorithm.^[4] To determine whether iPAIRs represented true immune synapses, we first used HiRes imaging to examine lobular iPAIRs identified on LoRes images from our archives. Slides selected were from six iWITH patients: two baseline eligibility biopsies (one from a patient tolerant of ISW, one patient nontolerant of ISW), four iWITH-IN 4-year follow-up biopsies. iPAIRs were identified from CD34/CD45/MHCII staining on a LoRes WSI via NearCYTE (<http://nearcyte.org/>) as one CD34⁻/MHCII⁺/CD45^{low/variable} (interpreted as CD45⁻) APC paired with one CD34⁻/MHCII[±]/CD45^{high} lymphocyte where the nuclei are separated by $\leq 5\mu\text{m}$ (Figure S2A).^[4,9] Although it is recognized that some APC, including Kupffer cells, display CD45 expression by flow cytometry,^[33] IHC staining for this marker in tissues results in a negative/low/variable expression, as is seen in the Human Protein Tissue Atlas.^[34] Therefore, we interpreted the Kupffer cells and other APC as CD45⁻ in comparison to the high expression seen in lymphocytes.

A total of 1167 iPAIRs were screened after random sampling across multiple biopsies for imaging. iPAIRs were excluded from HiRes imaging if on the LoRes image they fell into clusters of more than two cells (Figure S2B) or in portal regions (Figure S3) because of cell crowding and overlapping phenotype features. Using XY axis fiducial mapping (Figure S4), a total of remaining 183 lobular iPAIRs were then imaged at HiRes and adjudicated by two reviewers (M.W.T. and D.L.). Further exclusions were made if (1) the identified pairing had poor cellular morphology (Figure S2C), (2) the nucleus of the APC and/or lymphocyte could not be clearly defined and was abnormally shaped because of suboptimal nuclear segmentation (Figure S3C), or (3) the morphologic features of the lymphocyte nucleus could not be clearly resolved in NearCYTE. NearCYTE analysis of HiRes nuclei were segmented (identified), and morphometrics were evaluated on 98 iPAIRs and 41 excluded pairings that could be evaluated by NearCYTE. We defined objective metrics for cytoplasmic (Figure S5) and nuclear (Figure S6A) morphology characteristics of iPAIRs that correlated with defining features of immune synapse formation.^[8,14,35]

Distance between nuclei in lobular iPAIRs with HiRes imaging is $<0.5\mu\text{m}$

Using confocal microscopy (resolution at 0.27 μm per pixel), human kidney studies reported that closely packed T cells and APCs (T follicular helper cells to B cells) had nuclei that were 2–4 μm apart, whereas cells engaged in immune synapses had nuclei $<0.54\mu\text{m}$ apart.^[11,12] Lobular iPAIRs ($n = 98$) evaluated at HiRes (0.06 μm per pixel; Figure S6A) had a significantly smaller ($p = 0.036$) mean internuclear distance of 0.713 μm compared with excluded pairings whose mean internuclear distance was 1.250 μm ($n = 25$). Shortening the distance ($\leq 3\mu\text{m}$ at LoRes or $\leq 0.5\mu\text{m}$ at HiRes) between the nuclei of the MHCII⁺ and CD45⁺ cells in our classifier more selectively captures biological immune synapses.

Improved identification of immune synapses using automated image analysis

Following nuclear segmentation incorporating level set methods (Figure S6B), fully automated tissue-tethered cytometry was performed using NearCYTE (<http://nearcyte.org/>), as described.^[4,9] Additional constraints were applied to the iPAIR definition for Automated Image detection of Immune SYNapses (ai-iSYN) on LoRes WSIs. Ai-iSYNs are defined in Figure 2A. Clustering of MHCII⁺ cells are used to define lobular and portal regions of liver tissue, as previously described.^[9] Dilation and total coverage of cytoplasmic area by staining measures remain the same. Analysis was applied using automated batch processing without human intervention. Results detected by the new ai-iSYN classifier were compared with prior results from the iPAIR classifier using iWITH specimens (Figure S7).

Biologically active interactions between APC and lymphocytes with HiRes imaging

CD3/CD8/CD45/MHCII/CD34-stained FFPE slides were scanned at LoRes and subjected to ai-iSYN identification and mapped with fiducial markers for coordinate mapping and HiRes imaging (Figure S4). A total of 757 lobular ai-iSYNs from seven patient slides were evaluated. Patient slides included one iWITH baseline preweaning biopsy from a nontolerant patient with ISW, one iWITH-IN 4-year follow-up biopsy, and five ARTEMIS biopsies (3 screening biopsies, 2 biopsies from time of infusion). Ai-iSYNs were then selected for HiRes imaging after confirmation that (1) an identified lymphocyte-APC pair met the definition for a lobular ai-iSYN (Figure 2A) and (2) the lymphocyte of the pair was CD34⁻/CD3⁺/CD8^{any}/CD45^{High}.

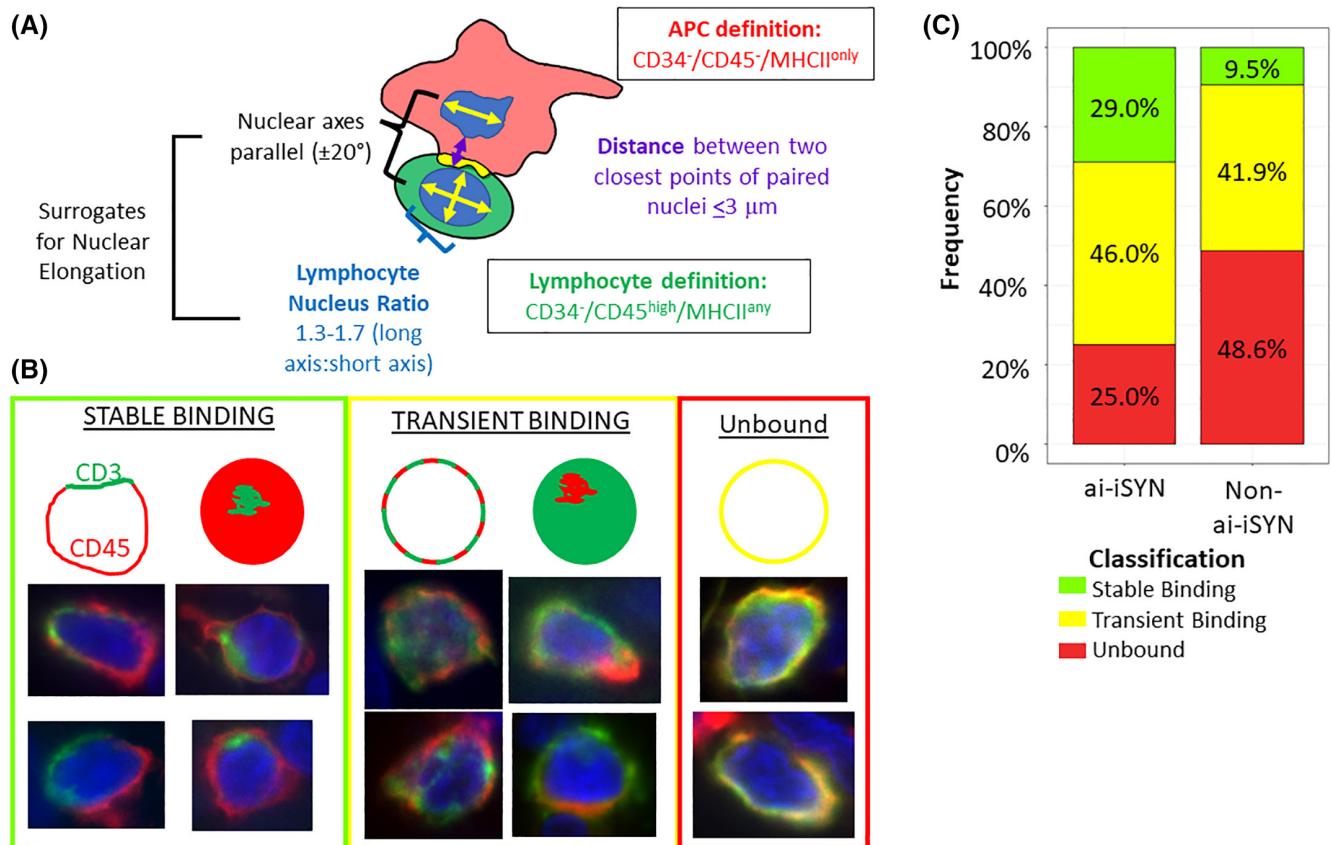


FIGURE 2 Definition of Automated Image detection of Immune SYNapses (ai-iSYNs) and representative phenotypes of actively bound immune synapses. (A) Biopsies were stained with a multiplex immunohistochemistry panel that combined CD45 (a pan lymphocyte marker), HLA-DPB1 (major histocompatibility complex [MHC] II expressed strongly on antigen-presenting cells [APCs]), CD8 (expressed by cytotoxic T cells, natural killer cells, cortical thymocytes, and some dendritic cells), MAC387 (calprotectin expressed by granulocytes, monocytes and recently immigrated tissue macrophages), and CD34 (endothelial cell marker). After low-resolution whole slide imaging, the refined ai-iSYN classifier (1) identified CD34⁺/CD45⁻/MHCII^{only} APCs paired with a CD34⁻/CD45^{high}/MHCII^{any} lymphocytes (as in the immune pair classifier); (2) included only pairs where the distance between the closest points of the paired nuclei is ≤ 3 μm; (3) confirmed that the long axes of the nuclei of the paired cells are parallel to each other ±20°; and (4) considered only pairs in which the lymphocyte nuclear ratio of long axis/short axis is 1.3:1.7, indicative of elongation. Nuclei with elongation >1.7 were excluded because the majority of these nuclei were suboptimally segmented with artificially created spurs. (B) Lobular lymphocytes identified (or not) by the ai-iSYN algorithm were evaluated for polarization of CD3 and CD45 from high-resolution images, including detection of supramolecular activation complex (SMAC) formation. The phenotype of the lymphocytes engaged in ai-iSYNs were defined based on binding stability depicted in published literature^[8,19,35–38]: “stable,” “transient,” or “unbound.” “Stable” lymphocytes have complete polarization of CD3 to one cytoplasmic location with CD45 exclusion from that region, indicative of SMAC formation. “Transient” lymphocytes have multiple clusters of CD3 in which CD45 is excluded giving the cytoplasm a speckled or spotted appearance. “Transient” lymphocytes may also have an inside-out phenotype in which a single patch of CD45 is present with CD3 exclusion. “Unbound” pairings do not have features of “stable” or “transient” pairings and show overlapping signal for CD3 and CD45. Lymphocytes not present in ai-iSYNs were also evaluated. Representative examples are shown. (C) Proportions of lobular lymphocyte phenotypes (in ai-iSYNs $n = 176$; not in ai-iSYNs $n = 148$) were plotted: “stable” (green), “transient” (yellow), “unbound” (red). The χ^2 analysis of the contingency table of binding stability shows significant difference between the paired and unpaired lymphocyte population ($p < 0.001$).

This yielded a total of 176 candidate ai-iSYNs, from which the corresponding lymphocyte was adjudicated by two reviewers (M.W.T. and A.G.) for evidence of polarization from HiRes images. Lymphocyte polarization was defined by published morphological descriptions of immune synapse formation^[8,19,35–38] as “stable,” “transient,” or “unbound” (Figure 2B). All pairings were classified as CD8⁺ or CD4⁺ (CD3⁺/CD8⁻). Comparisons were made between lobular lymphocytes in ai-iSYNs or not ($n = 176$ and 148, respectively).

Gene expression pathway analysis of iWITH data using biclustering and number of lobular ai-iSYNs/mm²

Gene expression analyses were conducted as part of the iWITH trial on 148 RNA samples from eligibility biopsies using the Nanostring nCounter platform.^[9] Raw data can be accessed via the Immune Tolerance Network TrialShare (https://www.itntrialshare.org/iWITH_primary.url). Analysis used biclustering techniques (Supporting Methods and Figure S8).

Operational tolerance prediction algorithm

Previously stained FFPE slides from all available iWITH eligibility biopsies were subjected to NearCYTE classification to evaluate lobular ai-iSYNs per square millimeter, total MAC387⁺ cells per square millimeter, and lobular CD8⁺ cells per square millimeter ($n = 57$). These parameters were plotted on a three-dimensional cube whereby the axes were normalized and scaled between 0 and 1 (mapped minimum and maximum value). Clinical endpoints from the iWITH trial were overlaid, allowing for identification of the thresholds that, simultaneously, maximize the number of tolerant subjects and minimize the number of nontolerant subjects. Thresholds were chosen based on evaluating an Receiver Operating Characteristic Classification Table, whereby true positive, true negative, false positive, and false negatives were calculated, and the chosen cutoffs were selected to maximize sensitivity and minimize specificity.

Statistics

All statistical calculations were performed using R (v4.0.3)/RStudio (v1.1.442; [RRID:SCR_000432](#)), via imported tabular data generated from the morphological and spatial analyses of the WSIs. When applicable, all numerical data associated with count or quantities were normalized by the tissue area (square millimeters). Comparisons between two groups for nuclear distance and nuclear elongation used Welch's *t*-test. Two-sample proportionality testing was used to compare the binding phenotypes between lymphocytes identified as part or not part of an ai-iSYNs and subcategories thereof. Comparisons among receiver operator curves for prediction performance of logistic regression modeling were performed via calculation of model residual deviance.

RESULTS

Algorithm improvement: lymphocyte nuclear elongation in lobular iPAIRs is discernable on LoRes images

During immune synapse formation, lymphocytes flatten as spreading over the APC surface facilitates intercellular binding and signaling activation.^[13,14,19] Because nuclear shape generally mimics cell shape,^[39] we reasoned that lymphocyte nuclear flattening should be a detectable morphological feature (Figure 1A, Supporting Methods). Nuclear flattening was evaluated by measuring each lymphocyte in a lobular iPAIR defined at LoRes to determine elongation versus compactness. The elongation metric differed between lobular lymphocytes participating versus not participating in iPAIRs (Feret diameter mean 2.1 [SD 1.77, SEM = 0.056] vs. 1.6 [SD 1.03, SEM = 0.033]; $p < 0.001$). The compactness metric similarly differed,

confirming that lobular lymphocytes participating in iPAIRs were less round than those that did not (mean 1.48 [SD 0.51, SEM = 0.016] vs. 1.37 [SD 0.28, SEM = 0.001]; $p < 0.001$). Together, these data confirm that software-detected lobular iPAIRs more frequently contain lymphocytes with flattened nuclei, when compared with non-iPAIR lymphocytes, indicative of physiological engagement with and activation by APCs. Nuclear elongation evaluated via LoRes imaging is an objective metric that can improve software-assisted detection of immune synapses.

Confirmation of active immune synapse biology

Building upon the original iPAIR classifier, a refined model for ai-iSYN was established (Figure 2A). The ai-iSYN classifier performed comparably to the iPAIR classifier, despite decreased numbers of immunologic pairings identified because of more selective constraints (Figure S7). We set out to confirm that lobular ai-iSYNs have biologically relevant features of immune synapses including SMAC formation and that detection of ai-iSYNs correlated with the expression of genes and gene pathways consistent with activation of immune responses (Figure 1B).

Lobular ai-iSYNs display polarization with SMAC formation and often contain CD8⁺ T cells

Lymphocytes engaged or not engaged in lobular ai-iSYNs were classified based on staining for characteristics of SMAC presence and thus “stable” binding between an APC and lymphocyte. The phenotype of the lymphocytes engaged in ai-iSYNs were defined based on binding stability depicted in published literature (Figure 2B).^[8,19,35–38,40,41] “Stable” lymphocytes have CD45 exclusion from sites of T cell receptor (TCR) complex formation, and CD3, a TCR found in the central region of the SMAC, is present in the CD45 exclusion zone (Figure 2B). “Transient” lymphocytes have multiple clusters of CD3 in which CD45 is excluded or may have an inside-out phenotype in which a single patch of CD45 is present with CD3 exclusion. “Unbound” pairings show overlapping signal for CD3 and CD45.

Of 176 adjudicated CD3⁺/CD45⁺ lobular ai-iSYNs evaluated at HiRes, lymphocytes in 29% ($n = 51$ of 176) had a discernable SMAC (Figure 2C). Of the remaining lymphocytes without SMAC formation, 46% ($n = 81$ of 176) displayed a “transient” phenotype and 25% ($n = 44$ of 176) displayed an “unbound” phenotype.^[19,35–37] In contrast, when CD3⁺/CD45⁺ non-ai-iSYNs were evaluated, only 9.5% ($n = 14$ of 148) had a discernable SMAC, 41.9% ($n = 62$ of 148) displayed a “transient” phenotype, and 48.6% ($n = 72$ of 148) displayed an “unbound” phenotype (Figure 2C). The χ^2 analysis of the

contingency table of binding stability shows significant difference between the paired and unpaired lymphocyte population ($p < 0.001$). These data indicate that ai-iSYN lobular lymphocytes have a physiological phenotype of SMAC formation with APCs. The large percentage of lobular lymphocytes with a “transient” phenotype is consistent with the probing and monitoring nature of T cells traversing the APC-lined sinusoids,^[36,38,42] the reported effects of T cell activation state, and the APC type in immune synapse dynamics.^[43,44]

A higher density of CD8⁺ T cells, drivers of effector mechanisms and TCMR, was associated with unsuccessful ISW.^[3,4,9,10] We confirmed that higher density of lobular CD8⁺ T cells was more strongly associated with unsuccessful ISW in iWITH (tolerant vs. nontolerant, $p = 0.0087$, Figure S9B) compared with total CD8⁺ cells in the biopsy ($p = 0.050$; Figure S9A). Furthermore, we characterized the subtype of the CD3⁺ T cells in the lobular ai-iSYNs evaluated at HiRes. Of the 176 adjudicated CD3⁺/CD45⁺ lobular ai-iSYNs, 45% ($n = 79$ of 176; defined as CD3⁺/CD8⁻) contained CD4⁺ T cells and 55% ($n = 97$ of 176) contained CD8⁺ T cells. This ratio significantly differs ($p = 0.045$) from unpaired lymphocytes, of which 56.1% (83 of 148) were CD4⁺ and 43.9% ($n = 65$ of 148) were CD8⁺. Of lobular ai-iSYNs with a “stable” phenotype, 39.2% ($n = 20$ of 51) contained a CD4⁺ T cell versus 60.8% ($n = 31$ of 51) with a CD8⁺ T cell ($p = 0.51$). Therefore, CD8⁺ T cells are more frequently engaged with lobular APCs than CD4⁺ T cells, supporting the idea that identification of lobular ai-iSYNs and lobular CD8⁺ cells using software-assisted methods correlates with physiologically relevant biology in allograft biopsies and the presence of alloimmune activation.

Biclustering of gene expression data seeded by number of lobular ai-iSYNs yields enrichment profile consistent with T cell activation

Gene expression data from all available iWITH trial eligibility biopsies ($n = 148$) were reanalyzed using bicluster-driven supervised analysis via seeding by the number of lobular ai-iSYNs per square millimeter

(Supporting Methods, Figure S8). The resultant top 20 genes were *IL2RG*, *LCP1*, *CD74*, *CD5*, *LTB*, *MICB*, *CD53*, *IDO1*, *GZMA*, *CD97*, *HLA-DMB*, *CCL19*, *LCK*, *HLA-DRA*, *TIGIT*, *PTPRC*, *CD48*, *CCR2*, *CCL21*, and *ENTPD1*. Among these, *IL2RG* is required for T cell maturation^[45]; *LCP1* is essential for stabilization of immune synapses^[46]; *CD74* is a key molecule in MHCII antigen processing and presentation, immunity, and inflammation^[47]; and CD5 regulates T cell activation for immune synapse formation.^[48] Enrichment analysis (Supporting Methods) yielded pathways related to complement activation, humoral immunity, MHC protein complex binding, and T cell activation (Table 1), consistent with the role of complement in enhancing T cell alloreactivity.^[49] Previous studies noted the development of de novo donor-specific antibody (DSA) and in those who experience rejection after ISW.^[4,50]

To determine if patients with DSA fell into a particular subgroup in relation to our bicluster analysis of multiplatform datasets (Figure 3), patient biopsies were ranked by strength of correlation to the established biclustering pattern (x axis), determined by increasing density of ai-iSYNs and similarity of gene expression profile (Supporting Methods and Figure S8). Biopsies were additionally stratified by gene expression (y axis). DSA information was then represented by shapes and shading. These data suggest that patients with higher DSA mean fluorescent intensity also have higher cumulative average gene expression for the top 20 genes identified above. The above observations further support that NGP tools can detect subclinical but physiologically relevant humoral alloimmune activity in biopsies prior to ISM or ISW that may inform personalization of IS management in a patient. In addition, integration of NGP information with other clinical data sets can provide insights into patient groupings within a defined pathology.

Quality assurance performance assessment of refined prediction parameters for clinical relevance

To determine whether the performance of our algorithm with enhanced features was altered with respect

TABLE 1 Enriched Gene ontology pathways identified by biclustering gene expression data seeded with lobular Automated Image detection of Immune SYNapses per square millimeter (p -value cutoff 0.05)

Gene ontology ID	Gene ontology terms	p -value
GO:0006958	Complement activation, classical pathway	0.0070
GO:0002455	Humoral immune response mediated by circulating immunoglobulin	0.019
GO:0006956	Complement activation	0.042
GO:0030449	Regulation of complement activation	0.042
GO:0023023	MHC protein complex binding	0.045
GO:0050870	Positive regulation of T cell activation	0.049

Abbreviation: MHC, major histocompatibility complex.

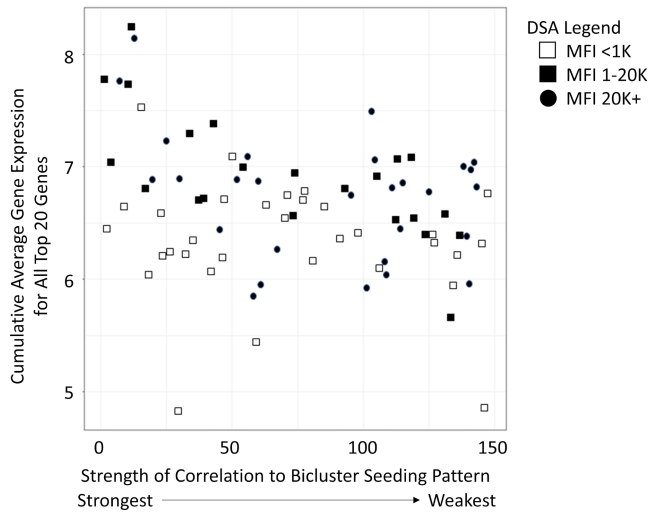


FIGURE 3 Biclustering of mRNA expression data based on the number of Automated Image detection of Immune SYNapses (ai-iSYN) per square millimeter allows for cross-platform data integration. Evaluation of iWITH mRNA expression data using supervised biclustering based on lobular ai-iSYN per square millimeter (histopathological data) to rank patients. Each symbol represents a single baseline eligibility biopsy (all eligible and ineligible iWITH patients). The x axis corresponds to the strength of correlation to the bicluster seeding pattern (0 = strongest). The y axis relates to the cumulative average gene expression for the top 20 genes (*IL2RG*, *LCP1*, *CD74*, *CD5*, *LTB*, *MICB*, *CD53*, *IDO1*, *GZMA*, *CD97*, *HLA-DMB*, *CCL19*, *LCK*, *HLA-DRA*, *TIGIT*, *PTPRC*, *CD48*, *CCR2*, *CCL21*, and *ENTPD1*) relative to control genes. To query the relationship to donor-specific antibody (DSA), symbols are used to correlate to the mean fluorescent intensity (MFI) value of DSA presence in the patient: open square = <1000; filled square = 1–20,000K; filled circle = 20,000+.

to the original classifier,^[4] as a quality assurance exercise, iWITH biopsies were used as a confirmation cohort. The algorithm's performance was specifically examined on eligibility biopsies of children who initiated ISW ($n = 53$). Slides previously stained for CD34/CD45/MHCII, MAC387, and CD8 (Methods) were reanalyzed to confirm that the algorithm's ability to predict successful ISW was not degraded (Figure 1C; Figure 4). The upgraded algorithm used enhanced nuclear segmentation and the density of lobular ai-iSYNs, lobular CD8⁺ T cells, and total MAC387⁺ cells and confirmed the detection of true immune synapses. The enhanced algorithm was not diminished. Instead, it performed with 87.3% accuracy, 100% sensitivity, and 75% specificity (CI: 81%–94%, 78%–100%, 56%–87%, respectively). This is in comparison to the original algorithm, which performed with 81.4% accuracy (94% sensitivity, 66% specificity).^[4] In Figure 4, the inner cube identifies thresholds that simultaneously maximize the number of tolerant patients (18 of 18; 100%) and minimize the number of nontolerant subjects (9 of 35, 25%). Thus, even after standard histologic evaluation, which excluded children with more than mild subclinical inflammation for ISW (as defined previously^[4,9]), this NGP

tool can predict, among eligible children who initiated ISW, those who succeeded or failed.

DISCUSSION

The most important conclusion of this study is the observation that automated image analysis software can objectively identify and quantify ai-iSYNs, which are intralobular pairings between lymphocyte and APCs with specific features indicative of biologically relevant immune synapses. In turn, the aiSYNs illustrate that intrahepatic T cell priming can occur in human liver lobules, similar to experimental animal models.^[5] Moreover, they are informative of the intrahepatic immune microenvironment. Increased density of lobular immune synapses likely represents the beginnings of an active allo-immune response (subpathological rejection), as evidenced by the development of clinical rejection after ISW.^[3] Therefore, it may be useful to guide IS decision-making.

Lymphocytes that were stably bound to APCs showed SMACs, characterized by segregation of CD3 and CD45.^[19,35–37,40,41] The presence and biological relevance of SMAC was cross-validated by additional quantitative and independent metrics including (a) close distance between lymphocyte and APC nuclei; (b) a change of lymphocyte nuclear shape for those in close proximity to an APC; and (c) enrichment of gene pathways related to immune synapse stabilization, antigen processing of MHC antigens, and T cell activation and maturation. Lobular density of ai-iSYNs was and remains the most influential parameter of our overall prediction algorithm. Although threshold values may appear small, one must consider that a biopsy captures approximately 1/50,000th of the total liver mass.^[51] Thus, 1–17 lobular ai-iSYNs per mm² on a single slice of a single biopsy equates to millions of interactions when extrapolated to the entirety of the liver, suggesting that mass action of the immune microenvironment in an allograft has global clinical management implications.

Similar to clinical practice in which multiplatform data (e.g., liver injury test, DSA results, IS drug levels, original disease, imaging studies, and biopsy findings) establishes diagnoses and guides clinical management, we employed biclustering to integrate routine histopathology, mIHC staining, serology, and mRNA expression profiles to gain further insights into the underlying biology. Grouping gene expression data according to the density of lobular ai-iSYNs enriched expression of genes associated and pathways (e.g., complement-mediated processes, T cell activation, MHC protein complex) associated with increased immune synapse formation. Previous studies have shown the relevance of complement in enhancing immune synapse formation and alloreactivity.^[49,52] In turn, ai-iSYN detection predicted successful versus failed ISW. Further studies

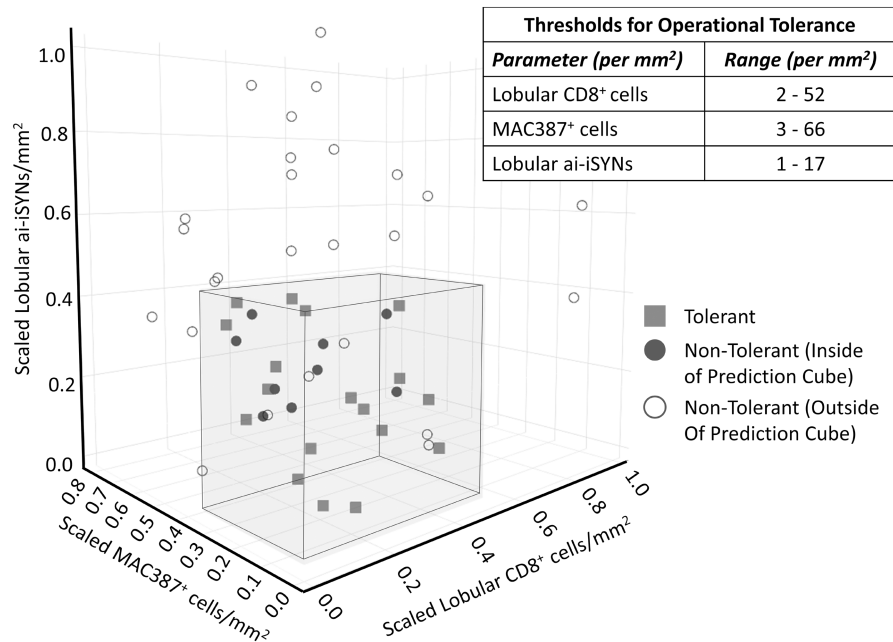


FIGURE 4 Use of multiplex immunohistochemistry parameters for prediction of operational tolerance from eligibility biopsies allows for separation of tolerant from nontolerant subjects. Shown in this three-dimensional scatter plot of tolerant (squares, $n = 18$) and nontolerant (circles, $n = 35$) patients according to the number of lobular CD8⁺ cells per square millimeter (T effector cells, x axis), MAC387⁺ cells per square millimeter (infiltrating macrophages, y axis), and lobular Automated Image detection of Immune SYNapses (ai-iSYNs) per square millimeter (z axis). Axes are scaled in which 0 is the lowest expression and 1 is the highest expression (see Methods). The inner cube (shaded box) identifies the inclusion thresholds that, simultaneously, maximize the number of tolerant subjects and minimize the number of nontolerant subjects. Ranges for the inner cube correspond to (1) lobular CD8⁺: 2–52 cells per mm²; (2) MAC387⁺: 3–66 cells per mm²; (3) lobular ai-iSYNs: 1–17 pairs per mm². Subjects within the inner cube are closed symbols; subjects outside the inner cube are open symbols.

are underway to iterate between biclustering analysis and protein expression in tissue sections to further support this line of reasoning.

The original classifier for identification of iPAIRs^[4,9] relied solely on a distance ($\leq 5 \mu\text{m}$) between paired nuclei. The refined ai-iSYN classifier incorporates evaluation of lymphocyte nuclear elongation, orientation of the lymphocyte nucleus to the APC nucleus, and a shorter distance between paired nuclei ($\leq 3 \mu\text{m}$) and enriches for immune synapse formation. Other algorithmic enhancements included implementation of level set smoothing after nuclear segmentation to provide a more accurate assessment of nuclear morphology by removal of spurious artifacts that would contort the nuclear shape. We also limited the CD8 parameter of the prediction algorithm to consider only lobular CD8⁺ cells rather than total CD8⁺ cells. Algorithmic changes were then quality assurance tested to determine performance. We confirmed that the enhanced ai-iSYN detection method further improved on the accuracy, sensitivity, and specificity of iPAIRs for prediction of successful ISW in a pediatric LTx cohort.

Future objectives to address limitations of our approach include (a) inclusion of events in portal tracts; (b) characterization of the subtypes of synaptically engaged T cells and/or MHCII lobular APC cells; and (c) dissemination of NGP capabilities. Pre-existing human and experimental animal data relevant to our

analysis^[3–6] support our current focus on lobular events. However, technical hurdles must overcome the challenges of cell crowding to incorporate portal events into our software-based prediction algorithm, particularly when dense portal inflammation is present. We also recognize that immune synapses are occurring in three dimensions, but this algorithm evaluates only a two-dimensional plane of view. We are unable to account for synapses that may be occurring between cells whose nuclei are $>3 \mu\text{m}$ apart or whose nuclei may be missing from the current focus plane. Therefore, this assay almost certainly underestimates the total number of synapses detected. However, the automated approach is unbiased with respect to study groups. Studies to more granularly phenotype synaptically engaged T cells and corresponding APCs (e.g., Kupffer cells, liver sinusoidal endothelial cells, and sinusoidal dendritic cells) are ongoing. Based on a combination of morphological features (stellate shaped cells located on top of liver sinusoidal endothelial cells), interrupted sinusoidal staining pattern, and the paucity of dendritic cells within the lobules, we hypothesize that most lobular ai-iSYNs identified in this study were between T cells and Kupffer cells, but a contribution from LSEC cannot be excluded.

In traditional anatomic pathology, a pathologist's attention is drawn to architectural landmarks (e.g., portal tracts and central veins) and/or clustering of inflammatory cells

for diagnosis of liver diseases (e.g., TCMR, autoimmune hepatitis, chronic hepatitis, etc.). This study shows that NGP techniques, when properly applied, (1) are a more sensitive and objectively quantitative method that can be used to understand underlying pathophysiology and (2) illustrate the importance of spatial context and intrahepatic events. This detailed characterization of the intrahepatic immune microenvironment effectively places a biopsy at one point along the spectrum of quiescent (“tolerogenic”) to active (“nontolerogenic”), a task that simply cannot be accomplished by routine biochemistry, serology, and/or routine histology. Moreover, arguably, this localization also cannot be accomplished by unsupervised mRNA clustering approaches.^[4] As such, NGP techniques may have clinical utility to guide IS decision-making through longitudinal surveillance of protocol biopsies (e.g., 3 and 5 years after transplantation). The spatial context at a submicron resolution scale and consequent mechanistic insights cannot be achieved by alternative noninvasive approaches.^[53] Our ultimate goal is to evolve this and related assays to guide personalized IS management for LTx recipients using equipment readily available in most clinical laboratories, thereby leveraging commercially available automated immunostaining devices, standard LoRes digital imaging, and open-source image analysis software.

Indeed, the ability of NGP, through precise and objective quantification of lobular aiSYNs, to accurately characterize the liver immune milieu provides a compelling rationale to incorporate protocol biopsies and NGP assessment, if ISM is considered. Performance validation in independent clinical populations will be the next critical step to advance this NGP tool for diagnostic use. Currently, efforts to determine whether NGP can predict the outcome of ISW for adult LTx recipients and ISM for autoimmune hepatitis patients are ongoing. NGP to characterize the presence and/or density of immune synapses may also be directly applicable to guide selection of immunotherapeutic agents to treat hepatocellular carcinoma.^[54] Finally, pathologists practicing NGP will be able to incorporate new approaches to tissue staining and software toolsets. Instead of front-line scoring and interpretation of biopsy findings, pathologists can pilot software to navigate a collection of relationships between and among various cell populations and tissue structures by applying a single rule set in an unbiased manner to all biopsies. The automated, objectively generated, data can then be integrated with data from other platforms to maximize a personalized approach to patient management.

AUTHOR CONTRIBUTIONS

Conceptualization: Michelle A. Wood-Trageser, Drew Lesniak, A. Jake Demetris, Sandy Feng, Alberto Sanchez-Fueyo, John Bucuvalas. Data curation, formal analysis, and software: Drew Lesniak; Funding acquisition: Michelle A. Wood-Trageser, A. Jake Demetris, Sandy Feng, Alberto Sanchez-Fueyo, John Bucuvalas.

Investigation: Michelle A. Wood-Trageser, Drew Lesniak, Alessandro Gambella, Kayla Golnoski. Methodology: Michelle A. Wood-Trageser, Drew Lesniak, Kayla Golnoski, A. Jake Demetris; Supervision: Michelle A. Wood-Trageser, A. Jake Demetris, Sandy Feng, Alberto Sanchez-Fueyo, John Bucuvalas. Validation: Michelle A. Wood-Trageser, Drew Lesniak. Visualization: Michelle A. Wood-Trageser, Drew Lesniak, Alessandro Gambella, A. Jake Demetris. Manuscript draft: Michelle A. Wood-Trageser, Drew Lesniak, A. Jake Demetris. Manuscript review, editing, final approval: all authors.

ACKNOWLEDGMENTS

The authors are grateful to the patients and their families who participated in the clinical trials. We wish to thank all of the iWITH, iWITH-IN, and ARTEMIS coinvestigators, research coordinators, and staff for their contributions to orchestration and execution of the various trials. Specifically, we thank Bryna Burrell, Allison Priore, Michael R. Narkewicz, Estella Alonso, George Mazariegos, Steve Lobritto, Elizabeth Rand, Vicky Ng, John Magee, Yumirle Turmelle, Nitika Gupta, Rhyam Himes, Michael Sheldon, Qizhi Tang, Jeffrey Bluestone, Sharon Blaschka, Crystal Lala, Kalpana Harish, Allan Kirk, Deborah Phippard, and Andre Hawkins for their contributions to planning, management, and administration of iWITH/iWITH-IN. We acknowledge the support received by the National Institutes of Health's National Center for Advancing Translational Sciences from the following institutions: University of California—San Francisco, San Francisco, California; Ann & Robert H. Lurie Children's Hospital of Chicago, Chicago, Illinois; Columbia University, New York, New York; Cincinnati Children's Hospital, Cincinnati, Ohio; Children's Hospital Colorado, Denver, Colorado; The Children's Hospital of Philadelphia, Philadelphia, Pennsylvania; St. Louis Children's Hospital, St. Louis, Missouri; and Emory University School of Medicine, Atlanta, Georgia.

FUNDING INFORMATION

Supported by the National Institute of Allergy and Infectious Diseases and National Institute of Diabetes and Digestive and Kidney Diseases (U01-AI-100807, R01 DK114180); Immune Tolerance Network (UM1AI109565), an international clinical research consortium headquartered at the Benaroya Research Institute and supported by the National Institute of Allergy and Infectious Diseases; and Clinical Trials in Organ Transplantation in Children (U01-AI-104347), a collaborative clinical research project headquartered at NIAID. Institutional support also provided by the Thomas E. Starzl Professor of Pathology Endowment at the University of Pittsburgh.

CONFLICT OF INTEREST

Sandy Feng owns stock in Johnson and Johnson. She consults for and received grants from Novartis.


A. Jake Demetris consults for and received grants from Novartis and Transmedics.

DATA AVAILABILITY STATEMENT

Raw gene expression data can be accessed via the Immune Tolerance Network TrialShare (https://www.itntrialshare.org/iWITH_primary.url). Data was previously published in Ref. 9 (Feng et al., 2018, *Gastroenterology*).


ORCID

Michelle A. Wood-Trageser  <https://orcid.org/0000-0002-1880-4926>

Alessandro Gambella  <https://orcid.org/0000-0001-7826-002X>

Sandy Feng  <https://orcid.org/0000-0002-2601-4350>

John Bucuvalas  <https://orcid.org/0000-0002-6767-8874>

Alberto Sanchez-Fueyo  <https://orcid.org/0000-0002-8316-3504>

A. Jake Demetris  <https://orcid.org/0000-0002-9582-3733>

REFERENCES

- Wood-Trageser MA, Lesniak AJ, Demetris AJ. Enhancing the value of histopathological assessment of allograft biopsy monitoring. *Transplantation*. 2019;103:1306–22.
- Wood-Trageser MA, Xu Q, Zeevi A, Randhawa P, Lesniak D, Demetris AJ. Precision transplant pathology. *Curr Opin Organ Transplant*. 2020;25:412–9.
- Wong T, Nouri-Aria KT, Devlin J, Portmann B, Williams R. Tolerance and latent cellular rejection in long-term liver transplant recipients. *Hepatology*. 1998;28:443–9.
- Feng S, Bucuvalas JC, Mazariegos GV, Magee JC, Sanchez-Fueyo A, Spain KM, et al. Efficacy and safety of immunosuppression withdrawal in pediatric liver transplant recipients: moving towards personalized management. *Hepatology*. 2021;73:1985–2004.
- Bénéchet AP, De Simone G, Di Lucia P, Cilenti F, Barbiera G, Le Bert N, et al. Dynamics and genomic landscape of CD8. *Nature*. 2019;574:200–5.
- Wong YC, Tay SS, McCaughan GW, Bowen DG, Bertolino P. Immune outcomes in the liver: is CD8 T cell fate determined by the environment? *J Hepatol*. 2015;63:1005–14.
- Gaudino SJ, Kumar P. Cross-talk between antigen presenting cells and T cells impacts intestinal homeostasis, bacterial infections, and tumorigenesis. *Front Immunol*. 2019;10:360.
- Garcia E, Ismail S. Spatiotemporal regulation of signaling: focus on T cell activation and the immunological synapse. *Int J Mol Sci*. 2020;21:3283.
- Feng S, Bucuvalas JC, Demetris AJ, Burrell BE, Spain KM, Kanaparthi S, et al. Evidence of chronic allograft injury in liver biopsies from long-term pediatric recipients of liver transplants. *Gastroenterology*. 2018;155:1838–51.e1837.
- Ronca V, Wootton G, Milani C, Cain O. The immunological basis of liver allograft rejection. *Front Immunol*. 2020;11:2155.
- Liarski VM, Kaverina N, Chang A, Brandt D, Yanez D, Talasnik L, et al. Cell distance mapping identifies functional T follicular helper cells in inflamed human renal tissue. *Sci Transl Med*. 2014;6:230ra246.
- Liarski VM, Sibley A, van Panhuys N, Ai J, Chang A, Kennedy D, et al. Quantifying in situ adaptive immune cell cognate interactions in humans. *Nat Immunol*. 2019;20:503–13.
- Lin W, Suo Y, Deng Y, Fan Z, Zheng Y, Wei X, et al. Morphological change of CD4(+) T cell during contact with DC modulates T-cell activation by accumulation of F-actin in the immunology synapse. *BMC Immunol*. 2015;16:49.
- Hivroz C, Saitakis M. Biophysical aspects of T lymphocyte activation at the immune synapse. *Front Immunol*. 2016;7:46.
- Tai Y, Wang Q, Korner H, Zhang L, Wei W. Molecular mechanisms of T cells activation by dendritic cells in autoimmune diseases. *Front Pharmacol*. 2018;9:642.
- Geiger B, Rosen D, Berke G. Spatial relationships of microtubule-organizing centers and the contact area of cytotoxic T lymphocytes and target cells. *J Cell Biol*. 1982;95:137–43.
- Ueda H, Morphew MK, McIntosh JR, Davis MM. CD4+ T-cell synapses involve multiple distinct stages. *Proc Natl Acad Sci U S A*. 2011;108:17099–104.
- Kupfer A, Dennert G. Reorientation of the microtubule-organizing center and the Golgi apparatus in cloned cytotoxic lymphocytes triggered by binding to lysable target cells. *J Immunol*. 1984;133:2762–6.
- Donnadieu E, Bismuth G, Trautmann A. Antigen recognition by helper T cells elicits a sequence of distinct changes of their shape and intracellular calcium. *Curr Biol*. 1994;4:584–95.
- Dustin ML, Olszowy MW, Holdorf AD, Li J, Bromley S, Desai N, et al. A novel adaptor protein orchestrates receptor patterning and cytoskeletal polarity in T-cell contacts. *Cell*. 1998;94:667–77.
- Philipsen L, Engels T, Schilling K, Gurbel S, Fischer KD, Tedford K, et al. Multimolecular analysis of stable immunological synapses reveals sustained recruitment and sequential assembly of signaling clusters. *Mol Cell Proteomics*. 2013;12:2551–67.
- Colin-York H, Javanmardi Y, Skamrahl M, Kumari S, Chang VT, Khuon S, et al. Cytoskeletal control of antigen-dependent T cell activation. *Cell Rep*. 2019;26:3369–79.e3365.
- Delon J, Bercovici N, Liblau R, Trautmann A. Imaging antigen recognition by naive CD4+ T cells: compulsory cytoskeletal alterations for the triggering of an intracellular calcium response. *Eur J Immunol*. 1998;28:716–29.
- Bein J, Thurner L, Hansmann ML, Hartmann S. Lymphocyte predominant cells of nodular lymphocyte predominant Hodgkin lymphoma interact with rosetting T cells in an immunological synapse. *Am J Hematol*. 2020;95:1495–502.
- Ben-Skowronek I, Szewczyk L, Ciechanek R, Korobowicz E. Interactions of lymphocytes, thyrocytes and fibroblasts in Hashimoto's thyroiditis: an immunohistochemical and ultrastructural study. *Horm Res Paediatr*. 2011;76:335–42.
- Ramsay AG, Clear AJ, Kelly G, Fatah R, Matthews J, Maccougall F, et al. Follicular lymphoma cells induce T-cell immunologic synapse dysfunction that can be repaired with lenalidomide: implications for the tumor microenvironment and immunotherapy. *Blood*. 2009;114:4713–20.
- Levitsky J, Burrell BE, Kanaparthi S, Turka LA, Kurian S, Sanchez-Fueyo A, et al. Immunosuppression withdrawal in liver transplant recipients on sirolimus. *Hepatology*. 2020;72:569–83.
- Kim M, Osborne NR, Zeng W, Donaghy H, McKinnon K, Jackson DC, et al. Herpes simplex virus antigens directly activate NK cells via TLR2, thus facilitating their presentation to CD4 T lymphocytes. *J Immunol*. 2012;188:4158–70.
- Derniame S, Vignaud JM, Faure GC, Béné MC. Alteration of the immunological synapse in lung cancer: a microenvironmental approach. *Clin Exp Immunol*. 2008;154:48–55.
- Demetris AJ, Isse K. Tissue biopsy monitoring of operational tolerance in liver allograft recipients. *Curr Opin Organ Transplant*. 2013;18:345–53.
- Gouw AS, Houthoff HJ, Huitema S, Beelen JM, Gips CH, Poppema S. Expression of major histocompatibility complex

- antigens and replacement of donor cells by recipient ones in human liver grafts. *Transplantation*. 1987;43:291–6.
32. Charlton M, Levitsky J, Aqel B, O'Grady J, Hemibach J, Rinella M, et al. International liver transplantation society consensus statement on immunosuppression in liver transplant recipients. *Transplantation*. 2018;102:727–43.
 33. Im M, Chae H, Kim T, Park HH, Lim J, Oh EJ, et al. Comparative quantitative analysis of cluster of differentiation 45 antigen expression on lymphocyte subsets. *Korean J Lab Med*. 2011;31:148–53.
 34. Uhlén M, Fagerberg L, Hallström BM, Lindskog C, Oksvold P, Mardinoglu A, et al. Proteomics. Tissue-based map of the human proteome. *Science*. 2015;347:1260419.
 35. Friedl P, den Boer AT, Gunzer M. Tuning immune responses: diversity and adaptation of the immunological synapse. *Nat Rev Immunol*. 2005;5:532–45.
 36. Kasprócz R, Rand E, O'Toole PJ, Signoret N. A correlative and quantitative imaging approach enabling characterization of primary cell-cell communication: case of human CD4. *Sci Rep*. 2018;8:8003.
 37. Turret M, Guégan S, Chemin K, Dogniaux S, Miro F, Bohineust A, et al. T cell polarity at the immunological synapse is required for CD154-dependent IL-12 secretion by dendritic cells. *J Immunol*. 2010;185:6809–18.
 38. Qi SY, Groves JT, Chakraborty AK. Synaptic pattern formation during cellular recognition. *Proc Natl Acad Sci U S A*. 2001;98:6548–53.
 39. Johnson GR, Buck TE, Sullivan DP, Rohde GK, Murphy RF. Joint modeling of cell and nuclear shape variation. *Mol Biol Cell*. 2015;26:4046–56.
 40. Hosseini BH, Louban I, Djandji D, Wabnitz GH, Deeg J, Bulbuc N, et al. Immune synapse formation determines interaction forces between T cells and antigen-presenting cells measured by atomic force microscopy. *Proc Natl Acad Sci U S A*. 2009;106:17852–7.
 41. Chang VT, Fernandes RA, Ganzinger KA, Lee SF, Siebold C, McColl J, et al. Initiation of T cell signaling by CD45 segregation at 'close contacts'. *Nat Immunol*. 2016;17:574–82.
 42. Blanchard N, Decraene M, Yang K, Miro-Mur F, Amigorena S, Hivroz C. Strong and durable TCR clustering at the T/dendritic cell immune synapse is not required for NFAT activation and IFN- γ production in human CD4⁺ T cells. *J Immunol*. 2004;173:3062–72.
 43. Azar GA, Lemaître F, Robey EA, Bousso P. Subcellular dynamics of T cell immunological synapses and kinapses in lymph nodes. *Proc Natl Acad Sci U S A*. 2010;107:3675–80.
 44. Underhill DM, Bassetti M, Rudensky A, Aderem A. Dynamic interactions of macrophages with T cells during antigen presentation. *J Exp Med*. 1999;190:1909–14.
 45. Kalman L, Lindegren ML, Kobrynski L, Vogt R, Hannon H, Howard JT, et al. Mutations in genes required for T-cell development: IL7R, CD45, IL2RG, JAK3, RAG1, RAG2, ARTEMIS, and ADA and severe combined immunodeficiency: HuGE review. *Genet Med*. 2004;6:16–26.
 46. Morley SC. The actin-bundling protein L-plastin: a critical regulator of immune cell function. *Int J Cell Biol*. 2012;2012:935173.
 47. Schröder B. The multifaceted roles of the invariant chain CD74--more than just a chaperone. *Biochim Biophys Acta*. 2016;1863:1269–81.
 48. Voisinne G, Gonzalez de Peredo A, Roncagalli R. CD5, an undercover regulator of TCR signaling. *Front Immunol*. 2018;9:2900.
 49. Lalli PN, Zhou W, Sacks S, Medof ME, Heeger PS. Locally produced and activated complement as a mediator of alloreactive T cells. *Front Biosci (Schol Ed)*. 2009;1:117–24.
 50. Shaked A, DesMarais MR, Kopetskie H, Feng S, Punch JD, Levitsky J, et al. Outcomes of immunosuppression minimization and withdrawal early after liver transplantation. *Am J Transplant*. 2019;19:1397–409.
 51. Bravo AA, Sheth SG, Chopra S. Liver biopsy. *N Engl J Med*. 2001;344:495–500.
 52. Cravedi P, van der Touw W, Heeger PS. Complement regulation of T-cell alloimmunity. *Semin Nephrol*. 2013;33:565–74.
 53. Vionnet J, Miquel R, Abraides JG, Wall J, Kodala E, Lozano JJ, et al. Non-invasive alloimmune risk stratification of long-term liver transplant recipients. *J Hepatol*. 2021;75:1409–19.
 54. Mokhtari RB, Sambhi M, Qorri B, Baluch N, Ashayeri N, Kumar S, et al. The next-generation of combination cancer immunotherapy: epigenetic immunomodulators transmogify immune training to enhance immunotherapy. *Cancers (Basel)*. 2021;13:3596.

SUPPORTING INFORMATION

Additional supporting information can be found online in the Supporting Information section at the end of this article.

How to cite this article: Wood-Trageser MA, Lesniak D, Gambella A, Golnoski K, Feng S, Bucuvalas J, Next-generation pathology detection of T cell–antigen-presenting cell immune synapses in human liver allografts. *Hepatology*. 2022;00:1–12. <https://doi.org/10.1002/hep.32666>